Bistatic Sensing and Multipath Mitigation with a 109-Element GPS Antenna Array and Digital Beam Steering Receiver

Kenn Gold, Alison Brown and Kees Stolk, *NAVSYS Corporation*

BIOGRAPHY

Kenn Gold is the Chief Technology Officer at NAVSYS Corporation. He previously was the Product Area Manager for the Advanced Systems and Simulation Tools group, and led the development of the Advanced GPS Hybrid Simulator. Prior to coming to NAVSYS, he was a Professional Research Associate at the Colorado Center for Astrodynamics Research. He received his PhD in Aerospace Engineering from CU Boulder in 1994.

Alison Brown is the President and Chief Executive Officer of NAVSYS Corporation. She has a PhD in Mechanics, Aerospace, and Nuclear Engineering from UCLA, an MS in Aeronautics and Astronautics from MIT, and an MA in Engineering from Cambridge University. In 1986, she founded NAVSYS Corporation. Currently, she is a member of the Interagency GPS Executive Board Independent Advisory Team (IGEB IAT), and an Editor of GPS World Magazine. She is an ION Fellow.

Kees Stolk is an engineer at NAVSYS Corporation working with simulation, design, and testing of NAVSYS advanced GPS systems including digital beam-steering, multipath estimation and reduction, and bistatic spatial signal processing. He has an MSc in Electrical Engineering from Twente University of Technology, Netherlands.

ABSTRACT

NAVSYS Corporation has developed a 109-element GPS antenna array and a modified version of the High-gain Advanced GPS Receiver (HAGR) which can perform beam steering with the digitally-combined signals from each antenna element. If adequate gain can be obtained from reflected GPS signals, applications involving Earth mapping, ocean surface mapping, terrain modeling, digital mapping, and other passive monitoring uses can benefit. Previous research in such uses of reflected GPS has been done at NAVSYS with a 16-element antenna array to sense the reflected signal. This paper describes the design of a 109-element Digital Beam-Steered Antenna Array and the collection of a data set to test the concept of operation.

The enhanced 109-element array provides 20 dB gain over single element tracking and offers promise of retrieving usable return data from a much higher altitude than previously possible for bistatic GPS remote sensing applications. Additionally, the directionality and high gain of the 109-element array will offer significant benefit in the mitigation of multipath error over conventional GPS receivers in normal terrestrial applications. Data analysis results from the proof-of-concept flight test with the array will be presented, along with pre-flight data for the next test. The flight data was collected with the antenna array placed on the bottom of an aircraft flying over the Gulf of Mexico.

INTRODUCTION

Early experimentation using NAVSYS' advanced GPS receiver technology demonstrated the ability to track the reflected GPS signals from the surface of the earth in the early 90s.[1] Since then, further research has demonstrated the utility of these signals for applications such as surface altimetry,[2] wave motion detection and wind sensing,[3] and observing surface water content[4,5] for mapping ice fields or wetlands.

Because of the extremely low-power level of the returned bistatic GPS signals, this previous research has focused primarily on the strong specular bistatic signals. NAVSYS has developed a digital beam steering GPS receiver, the High-gain Advanced GPS Receiver, which can be used to increase the received signal/noise ratio from these weak bistatic signal returns allowing improved detection of both specular and diffuse GPS signals.[6]

In this paper, the design of the HAGR is presented and results are included from a proof-of-concept flight experiment showing the improved bistatic signal processing possible when using this digital beam-steering receiver as a remote sensing instrument. Test results are also included showing the improved multipath rejection performance when using the 109-element GPS antenna array and Digital Beam Steering receiver.

DIFFUSE AND SPECULAR BISTATIC GPS SIGNALS

There are two types of bistatic GPS signals, diffuse and specular. Specular bistatic GPS signals are characterized by an optimal geometry, providing a very powerful reflection. Figure 1 shows the bistatic geometry and the specular points. The strength of the specular bistatic returns makes them easy to detect. The drawback, however, is the limited area of the earth's surface on which they provide information. The strength of the specular return depends on the smoothness of the surface. A smooth surface such as water provides much stronger specular returns than a rough surface such as forest.

Diffuse bistatic returns are produced by scattering of the GPS signal on the surface of the earth. Figure 1 shows that diffuse signal returns originate from a much larger area which could potentially provide information over a much larger region than possible by processing just the specular returns. However, these signals are extremely weak and require advanced receiver technology in order to be useful for remote sensing applications.

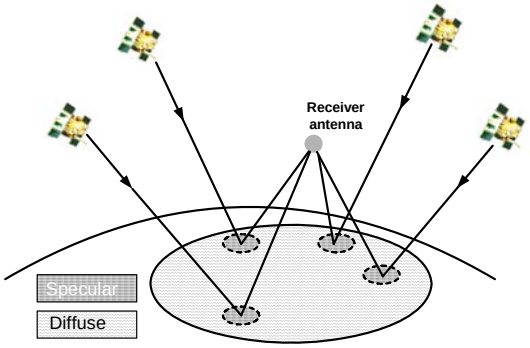

Figure 1 GPS Bistatic Geometry with Specular Reflection Points

RANGE/DOPPLER BISTATIC GPS SIGNAL PROCESSING

Figure 2 shows an example of a diffuse bistatic GPS scenario. The aircraft receives the direct signal from the satellite traveling along the line of sight. The GPS bistatic antenna receives a diffuse reflection from the earth surface. For each point on the surface of the earth, the bistatic signal return is received with a range and Doppler offset relative to the aircraft. This information can be used to distinguish between bistatic signal returns from different points on the earth.

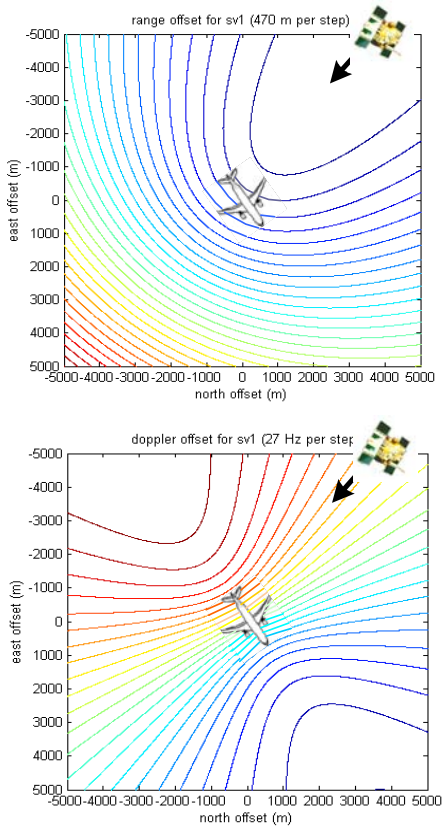

Figure 2 Equi-Range and Equi-Doppler Contours

The Doppler frequency of the bistatic signal relative to the direct signal, Δf (Hz), is computed as follows:

Equation 1

$$\Delta f_{\vec{x}} = \frac{\vec{v}_a \bullet \vec{k}_{\vec{x}} - \vec{v}_a \bullet \vec{k}_{sat}}{\lambda_{L1}}$$

Where

$\vec{v}_a$	aircraft speed (m/s)
$\vec{x}$	location where scattering occurs
$\vec{k}_{\vec{x}}$	line of sight from aircraft to scattering,
$\vec{k}_{sat}$	line of sight from aircraft to satellite
λ_{L1}	GPS L1 wavelength (m)

The following expression describes the range of the bistatic return signal, $\Delta\tau$ (m), relative to the direct signal:

Equation 2

$$\Delta\tau = \left\|\vec{x}_a - \vec{x}\right\| + \left(\vec{x} - \vec{x}_a\right) \bullet \vec{k}_{sat}$$

Where

$\vec{x}_a$	location of aircraft

It should be noted that a particular range/Doppler pair does not correspond to a unique 3-D point in space, but to a "slice" that can be represented by the intersection of the two surfaces shown in Figure 3. A constant Doppler region creates a cone around the aircraft's speed vector, while constant range maps to an ellipsoid. The combination results in an ambiguity curve of possible locations from which range/Doppler bistatic return can come from. This ambiguity can be resolved if surface altitude is known. The HAGR digital beam steering receiver also allows focusing on a bistatic return from a certain location by the use of range selection, Doppler selection and also beam steering to assist in resolving this region of ambiguity.

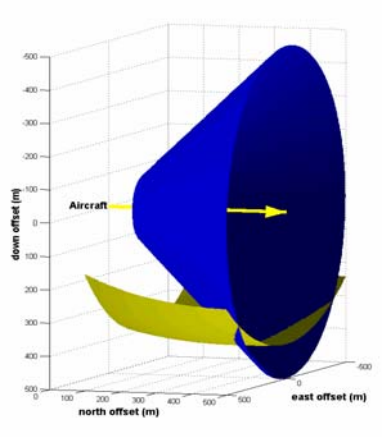

Figure 3 Diffuse Return Range/Doppler Ambiguity

BISTATIC SIGNAL/NOISE RATIO

In order to detect the weak GPS bistatic signal returns, advanced signal processing is needed to increase signal/noise ratio to an acceptable detection level. The amount a scatterer contributes to a bistatic return depends on the difference between selected range and Doppler and those of the scatterer, and its distance to the beam center. This is captured in a mathematical expression:

Equation 3

$$SNR = \frac{C}{N_0} \cdot T \cdot \iiint_V F_C^2(\vec{x}) \cdot F_D^2(T, \vec{x}) \cdot F_B^2(\vec{x}) \cdot \frac{\sigma}{4\pi R^2} d\vec{x}$$

Where

C/N_0	carrier to noise power ratio (dBHz)
T	coherent integration time (s)
F_C	range filtering action
F_D	doppler filtering action
F_B	beam steering
σ	radar cross section coefficient (m^2/ m^2)
R	range from plane to ground location (m)

The range filtering action depends on the geometry of the situation and the GPS code chip length. As shown in Figure 2, the area passed through the range filter forms a contour on the earth's surface. Equation 4 describes the range filter. Since this is a function of the chip length, there is a significant advantage to using the P(Y) code GPS signals for this processing which have 1/10th the chip length of the C/A code signals. The HAGR is able to track both the C/A and P(Y) code signals for approved users, and its reprogrammable architecture allows it to be upgraded for use with the future civil signals which also will have smaller chip sizes than the 1.023 MHz C/A code. The new L5 civil code planned for the Block IIF GPS satellites will have a 10.23 MHz chip rate.

Equation 4

$$F_C(\vec{x}) = \max\left(1 - \frac{\left|\tau_{\vec{x}} - \tau_{\vec{x}_0}\right|}{L_{chip}}, 0\right)$$

Where

$\tau_{\vec{x}_0}$	range offset at focus point
$\tau_{\vec{x}}$	range offset at point scattering
L_{chip}	the chip length for the GPS code

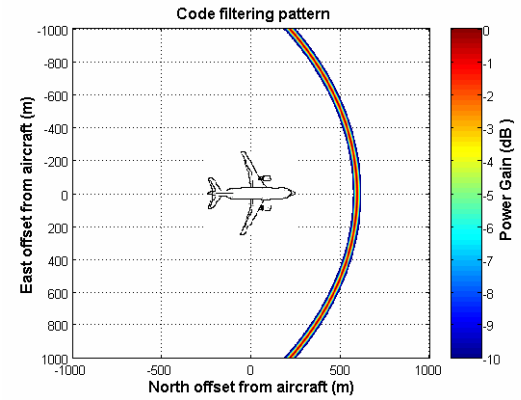

Figure 4 Range Filtering

The Doppler filtering action passes an area shown by the curve in Figure 2. The width of this "strip" depends on the coherent integration time T (Equation 5). The coherent integration time is chosen to roughly match the range filter width.

Equation 5

$$F_D(T, \vec{x}) = \left|\mathrm{sinc}\left(f_{\vec{x}_0} T - f_{\vec{x}} T\right)\right|$$

Where

$f_{\vec{x}_0}$	doppler offset at focus point
$f_{\vec{x}}$	doppler offset at point of scattering

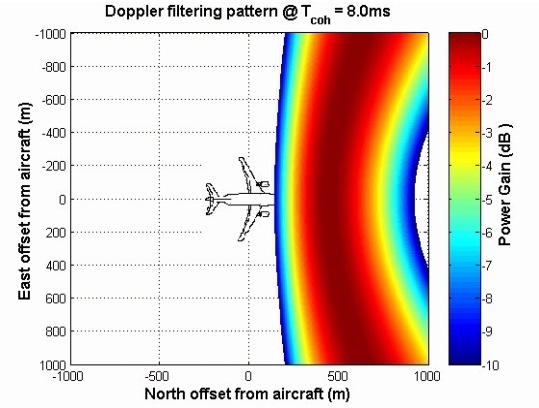

Figure 5 Doppler Filtering

The digital beam steering provides both gain and directional selectivity to resolve ambiguities. The signal gain depends on the number of elements (Equation 6). The HAGR can be configured with a variable number of antenna elements up to a total of 109-elements, as shown in Figure 6. For the proof-of-concept flight test, a 15-element array was used, with the elements shown in red in Figure 6. Figure 7 and Figure 8 shows the 15-element and 109-element beam pattern created by this array. Through the HAGR digital control, these beams can be directed at any point on the surface of the earth for data collection. The area they cover is a function of the beam width and the aircraft altitude.

Equation 6

$$F_B\left(\vec{x}\right) = \frac{\left|\vec{e}_{\vec{x}_0}^{H}\vec{e}_{\vec{x}}\right|}{\sqrt{M}}$$

M number of antenna elements

$\vec{e}_{\vec{x}_0}$ steering vector at focal point

$\vec{e}_{\vec{x}}$ steering vector at point of interest

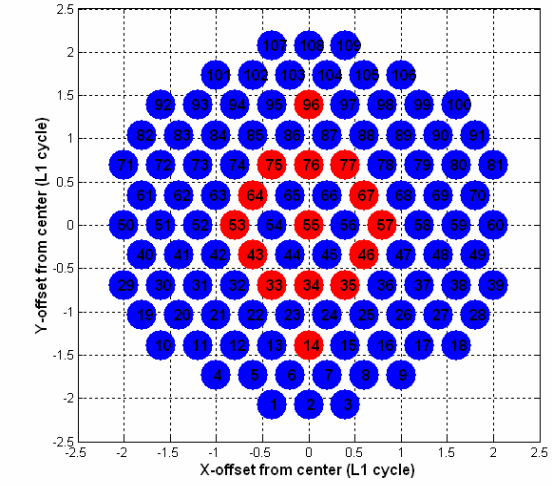

Figure 6 15 and 109-Element Phased Array

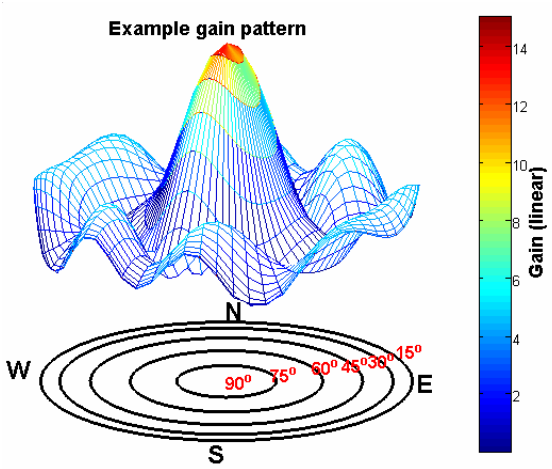

Figure 7 Beam Pattern of 15-Element Phased Array

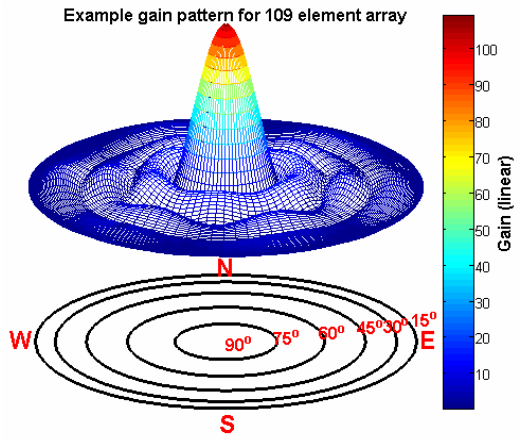

Figure 8 Beam Pattern of 109-Element Array

DIGITAL BEAM-STEERING GPS RECEIVER

The NAVSYS HAGR is a digital beam steering receiver designed for GPS satellite radio navigation and other spread spectrum applications. This is available for both military and commercial precision GPS applications and is installed in a rugged Compact PCI chassis which can be configured for either rack mount (Figure 9) or ATR (1½ LRU) installation for aircraft flight tests.

The HAGR system architecture is shown in Figure 10. The signal from each antenna element is first digitized using a Digital Front-End (DFE). Each DFE card includes the capability to sample signals from 8 antenna inputs. These can be cascaded together to allow beam-steering to be performed from a larger antenna array. The complete set of DFE digital signals is then used to create the composite digital beam-steered signal input by applying a complex weight to combine the antenna array outputs. Up to 12 beams can be independently directed by the HAGR signal processing.

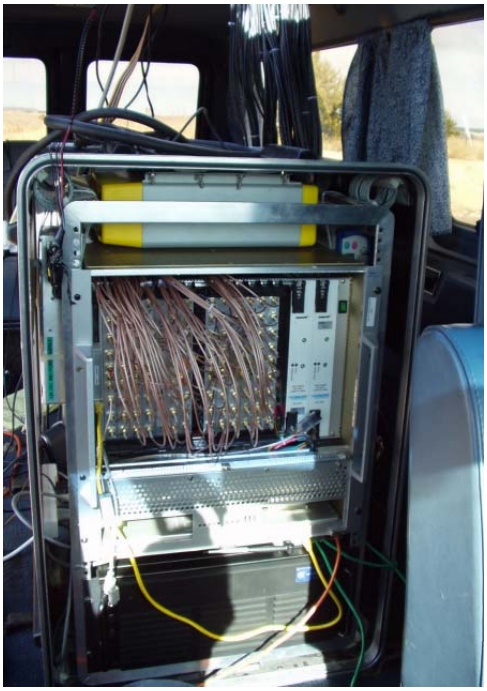

Figure 9 HAGR Assembly shown with Digital Storage Receiver

The HAGR can track up to 12 satellites simultaneously. In the normal mode of operation, the beams follow the satellites as they move across the sky (Figure 11). For bistatic signal processing, the beams can be directed at any particular point of interest on the earth. The array weights are applied independently for each of the HAGR signal processing channels which allows the antenna array pattern to be pointed in any direction through software control.

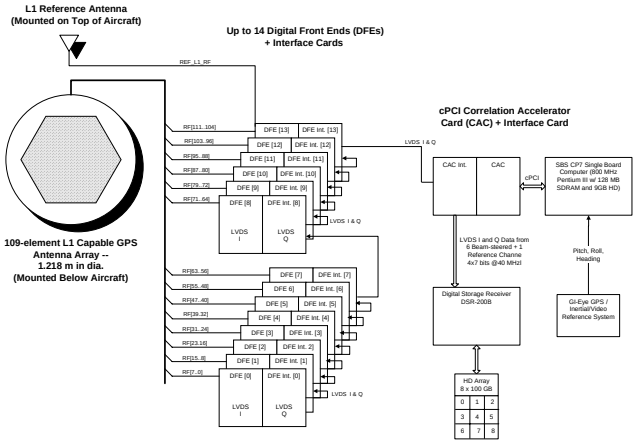

Figure 10 HAGR 109 element System Architecture

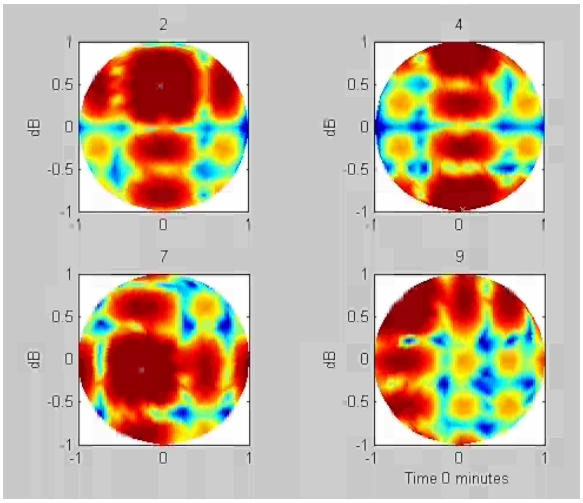

Figure 11 Satellite Beam Steering Mode

BISTATIC PROOF-OF-CONCEPT GPS FLIGHT TEST

The first flight test was conducted with the 15-element digital beam steering GPS bistatic sensing system shown in Figure 12. This was installed on the under-side of a Cessna test aircraft and a reference antenna was installed on the upper-side of the aircraft. During this flight test, the HAGR was used to track the GPS satellites and the raw broadband data was also recorded from each of these elements, and a reference antenna using our Advanced GPS Hybrid Simulation (AGHS) digital storage capability.[7,8] Approximately one hour of bistatic maritime data and two hours of bistatic land data was collected. Using the AGHS, this was then played back into the HAGR for signal processing post-test.

Figure 12 Cessna Test Aircraft and Antenna Array Mounted underneath

To instrument the test, we also installed in the aircraft our GI-Eye GPS/inertial/video georegistration system.[9,10] This recorded the scenes from below the aircraft for use as a truth reference. The precision georegistration capability of this system also allowed targets of opportunities to be precisely geolocated within the imagery for use in post-test analysis of their corresponding bistatic GPS signatures. Figure 13 shows the view from under the aircraft of come of the land and ocean data collected from the GI-Eye during this flight test.

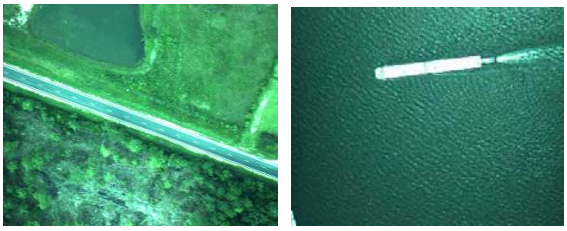

Figure 13 Land and Maritime surface

SPECULAR DATA ANALYSIS

Analysis of the specular return over land can be used to provide information on both elevation[2] and also the land-type where the signal is being returned (e.g. water content)[4,5]. For example, Figure 14 shows a dramatic increase in return power when the specular point crosses the Pearl River in a forest on the Mississippi-Louisiana border. The rough surface formed by the treetops provides a low specular return whereas the smooth river surface provides a very strong return.

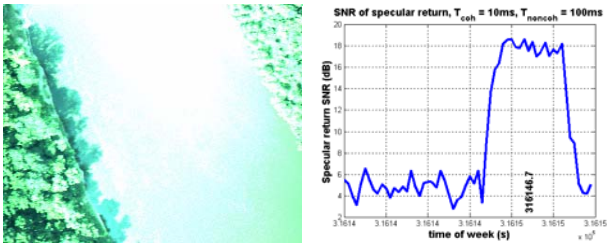

Figure 14 Pearl River Crossing, Specular Power Increase

LAND DIFFUSE DATA ANALYSIS

The recorded data was also analyzed to evaluate the magnitude of the diffuse bistatic GPS returns over land. This data was also used to build a GPS bistatic signal simulation tool for use in predicting the magnitude of the bistatic signatures as a function of the signal geometry and the modeled land clutter coefficients.

Because of the low level of the signal returns, reliable bistatic signal detection is only possible with the 15-element array over the region encompassing the range/Doppler boundary which maps to the hoop return shown in Figure 15. The Matlab model-based simulation tool was used to predict the area of coverage over which bistatic GPS signals could be expected to be detected for the 109 element antenna array which will be used in the next scheduled flight test. From Figure 16, this predicts that a much larger region of interest is covered using this larger version of the phased array which will open up some interesting new opportunities for remote sensing applications.

The 109-element HAGR is designed so that bistatic data can be collected using eight beams which are independently steered under software control. These are used to direct the antenna array gain towards either the specular regions associated with each satellite, as shown in Figure 17 or to collect data over the diffuse signal region as shown in Figure 18.

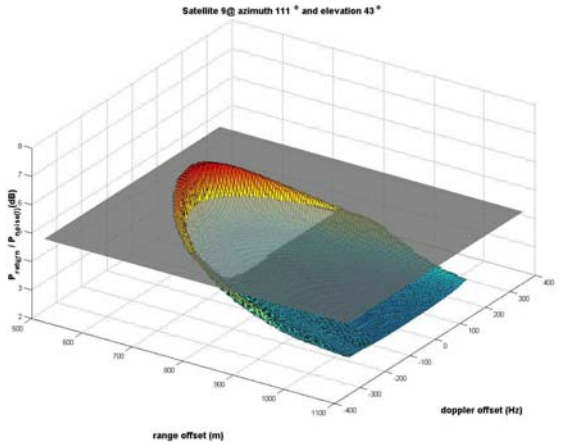

Figure 15 Modeled Bistatic Signals SV 9 (SNR Peak=7 dB)

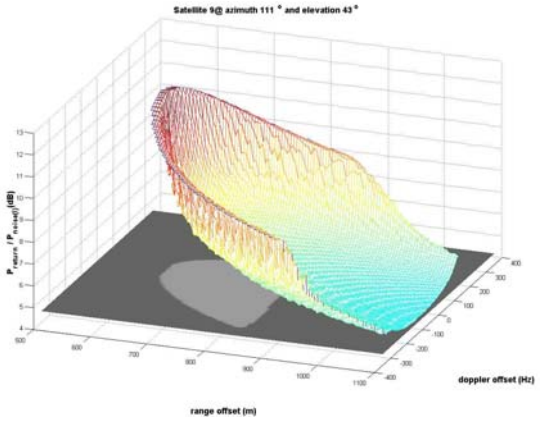

Figure 16 Simulation for 109 element array (SV 9)

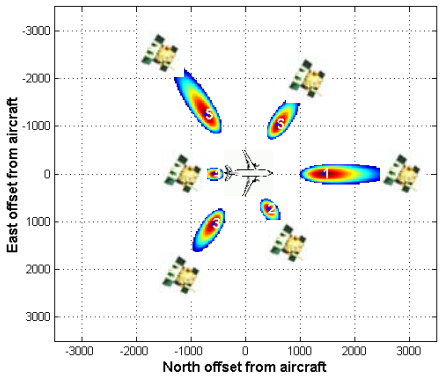

Figure 17 3dB Footprints towards Specular Point at 500 m Altitude

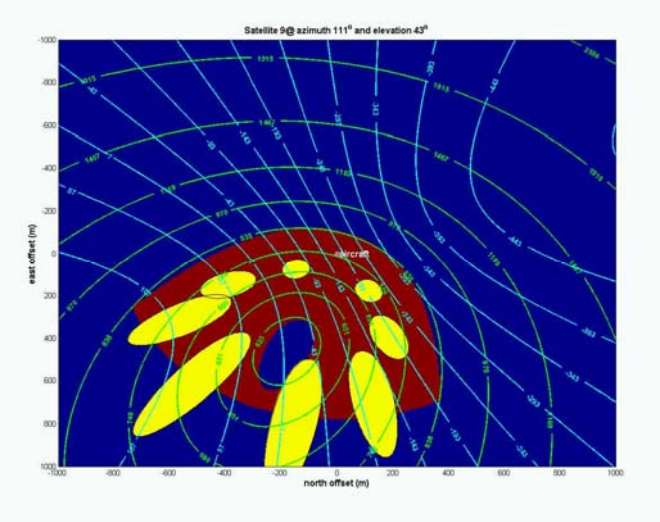

Figure 18 3dB Footprint Pattern for Diffuse Bistatic Signals

PRE-FLIGHT DATA COLLECTION WITH 109 ELEMENT ARRAY

In order to verify system functionality for the upcoming flight test with the 109 element array, the system was installed in a van, and data was collected at the NAVSYS location. Figure 19 shows the fully populated array, and the van used in this testing. The HAGR receiver and Digital Storage Receiver were located inside of the vehicle.

Figure 19 109 element array installed for van testing

Figure 20 shows the beam-steering results from this collected data. One beam was formed with data from a single element, while five other beams were formed with data from all elements. From the figure, it is apparent that the beams are achieving the expected 20 dB Gain.

Figure 21 and Figure 22 show the 10 msec coherent C/A correlation peaks from this collected data. As seen in Figure 22, the cross correlations of the C/A code between satellites shows significant power with the 109 element array which would result in false-locks occurring due to the cross-correlation between strong (e.g. specular) and weak (e.g. diffuse) signal returns.

The HAGR is capable of operating using both the C/A code and the secure P(Y) code signals. As shown in Figure 23, the P(Y) code does not exhibit the undesirable cross-correlation features of the C/A code and so provides better low power signal detection for the bistatic signal processing. The raw data recorded from the reference antenna on top of the aircraft is recorded with the Digital Storage Receiver, and played back into a keyed HAGR in the NAVSYS lab to capture the P(Y) code used to process the bistatic return.

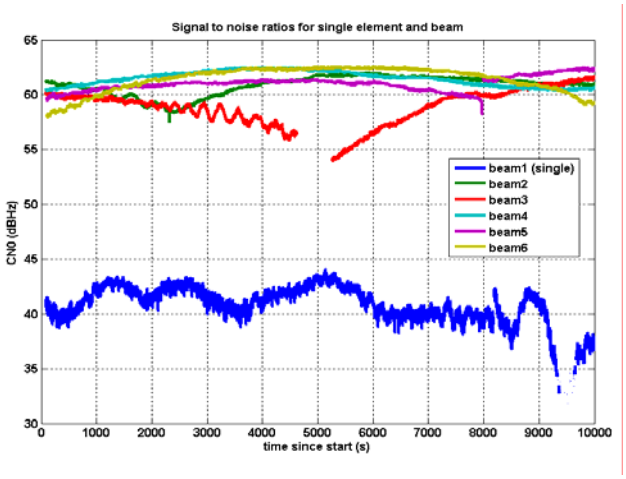

Figure 20 Beam steering results with the 109 element array

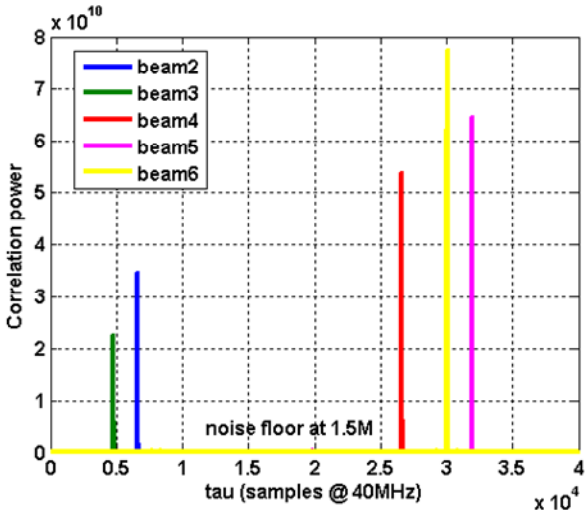

Figure 21 Ten msec correlation peaks for each beam

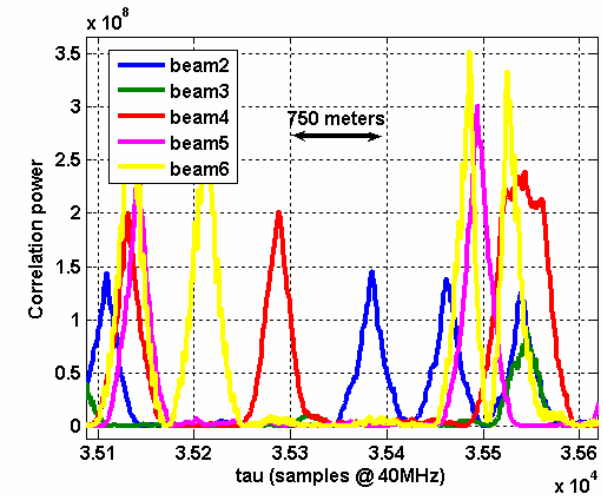

Figure 22 C/A Code Cross Correlations (False peaks)

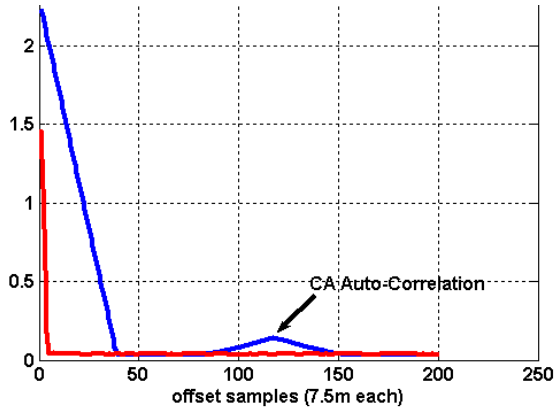

Figure 23 Comparison of P(Y) and C/A Correlation Peaks

MULTIPATH MITIGATION WITH 109 ELEMENT ARRAY

The increased gain associated with digital beam steering from 109 element array also significantly reduces the effect of multipath error on the received signals. The pseudorange multipath error can be quantified by looking at the code minus carrier (CMC) observable from the data. When these data types are differenced, the result is an observable containing ionosphere error, receiver noise, and multipath error. Figure 24 shows the CMC for the 109 element beam steering array, while Figure 25 shows the observable for a 7 element array. It is obvious from these figures that the multipath contamination is greatly reduced with the 109 element results.

The magnitude of multipath error on the carrier phase data can be observed by analyzing the fluctuations in the measured signal-to-noise ratios of the observed signals. Larger fluctuations imply larger multipath error. Figure 26 shows the C/No values for 109 elements, while Figure 27 shows these values for data collected with a 7 element array. Again, from these figures, it is apparent that the multipath error is significantly reduced with the 109 element array

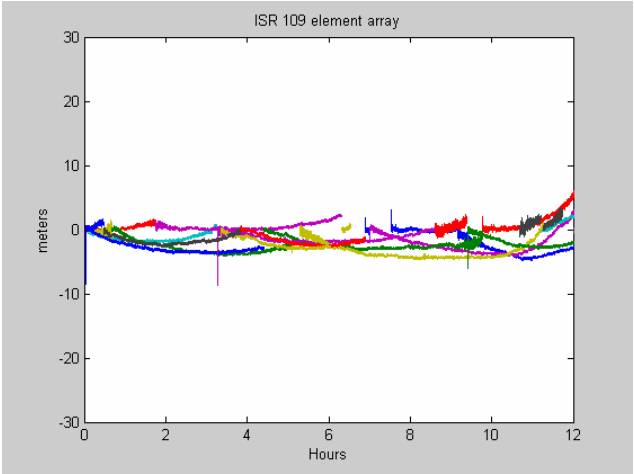

Figure 24 CMC observable with 109 element beams

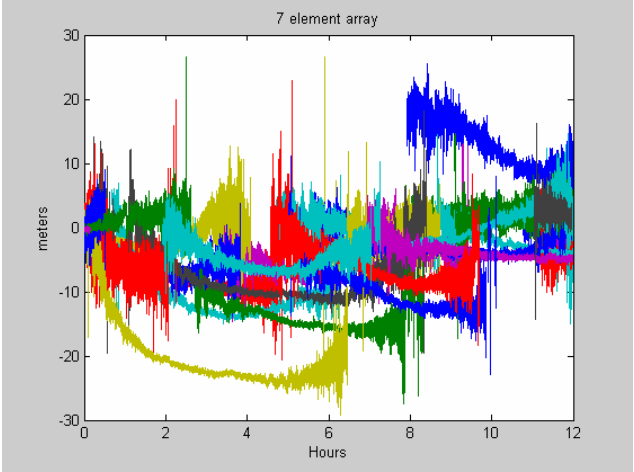

Figure 25 CMC observable with 7 element array

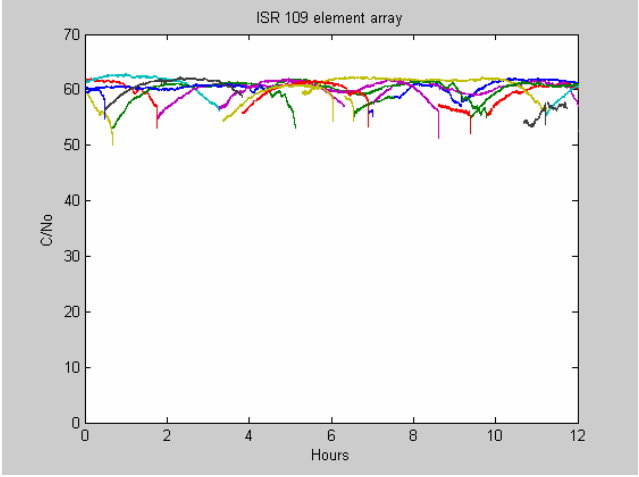

Figure 26 C/No values from the 109 element array

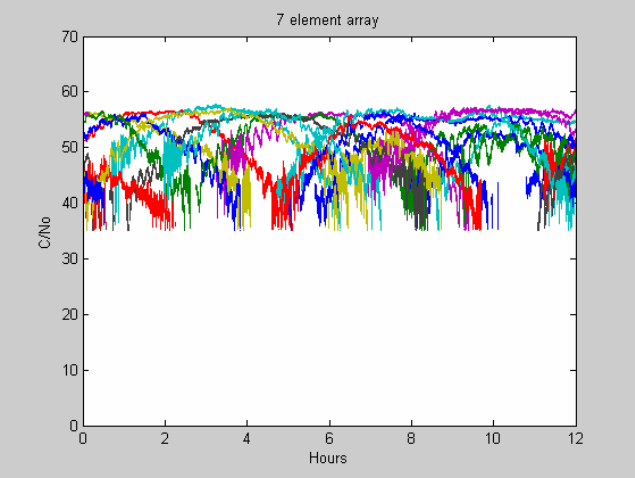

Figure 27 C/No values from a 7 element array

CONCLUSION

The test results and analysis described in this paper have demonstrated the ability of the HAGR receiver to improve the GPS bistatic remote sensing capability by using a Digital-Beam-Steered to allow weak GPS signal returns to be detected. The flight test results collected using a 15-element Digital-Beam-Steered phased array were used to demonstrate the following performance improvements possible with this receiver design.

- Robust detection and tracking of specular signals over both land and water
- Detection of diffuse signal returns over water from some surface vessels where backscatter occurred
- Detection of diffuse signal returns over a region of interest over land

We are currently in the process of assembling a 109 element phased array for the next flight test which is currently scheduled for February of 2005. This will provide the ability to boost the received bistatic signal returns by +20 dB gain using eight software controlled beams. We plan to collect more test data during this flight using these beams directed to both the specular return points and covering the diffuse region of interest. This +20 dB beam-steering capability is expected to further improve GPS bistatic signal analysis both by increasing the signal gain and also by removing range/Doppler ambiguity effects from the signal returns through the small beam-footprint.

ACKNOWLEDGEMENTS

The authors would like to acknowledge the support of Charles Luther of Office of Naval Research for sponsoring this activity. This work was funded under SBIR Contract No. N00014-00-C-0552.

REFERENCES

[1] J. Auber et al, "Characterization of Multipath on Land and Sea at GPS Frequencies", Proceedings of the Institute of Navigation GPS-94 Conference, Salt Lake City, Utah

[2] D. Masters, P. Axelrad, V. Zavorotny, S.J. Katzberg, and F. Lalezari, "A Passive GPS Bistatic Radar Altimeter for Aircraft Navigation," *ION GPS-2001*, Salt Lake City, OR, p. 2435-2445, September 2001

[3] V. U. Zavorotny, "Bistatic GPS Signal Scattering from an Ocean Surface: Theoretical Modeling and Wind Speed Retrieval from Aircraft Measurements," Workshop on Meteorological and Oceanographic Applications of GNSS Surface Reflections: from Modeling to User Requirements, July 6, 1999, De Bilt, The Netherlands, http://www.etl.noaa.gov/~vzavorotny/

[4] J. Garrison, S. Katzberg, "The Application of Reflected GPS Signals to Ocean and Wetland Remote Sensing," Proceedings of the Fifth International Conference on Remote Sensing for Marine and Coastal Environments, San Diego, CA, 5-7 October, Vol. 1, pp. 522-529, 1998.

[5] Masters, D, et al, "GPS Signal Scattering from Land for Moisture Content Determination", http://www-ccar.colorado.edu/~dmr/doc/pubs/files/igarss_soil_final.pdf

[6] K. Stolk and A. Brown, "Bistatic Sensing with Reflected GPS Signals Observed With a Digital Beam-Steered Antenna Array", Proceedings of ION GPS/GNSS 2003, Portland, OR, Sept. 2003

[7] A. Brown and N. Gerein, "Advanced GPS Hybrid Simulator Architecture", Proceedings of ION 57th Annual Meeting 2001, Albuquerque, NM, June 2001

[8] http://www.navsys.com/Products/aghs.htm

[9] D. Sullivan and A. Brown, "High Accuracy Autonomous Image Georeferencing Using a GPS/Inertial-Aided Digital Imaging System", Proceedings of ION National Technical Meeting 2002, San Diego, CA, Jan. 2002

[10] http://www.navsys.com/datasheets/NAVSYS_Gi-Eye.pdf